





Article

The Effect of Arsenic on the Photocatalytic Removal of Methyl Tet Butyl Ether (MTBE) Using Fe₂O₃/MgO Catalyst, Modeling, and Process Optimization

Akbar Mehdizadeh¹, Zahra Derakhshan², Fariba Abbasi¹, Mohammad Reza Samaei^{1,*},
Mohammad Ali Baghapour¹, Mohammad Hoseini¹, Eder Claudio Lima³ and Muhammad Bilal^{4,*}

¹ Department of Environmental Health Engineering, School of Health, Shiraz University of Medical Sciences, Shiraz 7153675541, Iran

² Research Center for Health Sciences, Department of Environmental Health, School of Health, Shiraz University of Medical Sciences, Shiraz 7153675541, Iran

³ Institute of Chemistry, Federal University of Rio Grande do Sul (UFRGS), Porto Alegre 91501-970, Brazil

⁴ School of Life Science and Food Engineering, Huaiyin Institute of Technology, Huai'an 223003, China

* Correspondence: mrsamaei@sums.ac.ir (M.R.S.); bilaluaf@hotmail.com (M.B.)

Abstract: MTBE is an aliphatic matter successfully removed from contaminated water by an advanced oxidation process. Additionally, arsenic is a toxic metalloid that is detected in some water supplies, such as in Iran. Concerning the oxidation potential of arsenic in an aqueous solution, it is expected that its interference in the photocatalytic removal of organic matter includes MTBE. Nevertheless, there is a lack of observation of this effect. In this study, the effect of arsenic on the photocatalytic removal of MTBE using an Fe₂O₃/MgO catalyst under UV radiation was investigated. Using an experimental design, modeling, and optimizing operational parameters, such as the arsenic and MTBE concentrations, catalyst dosage, pH, and reaction time, were studied. The synthesized nanocatalyst had a uniform and spherical morphological structure and contained 33.06% Fe₂O₃ and 45.06% MgO. The results indicate that the best model is related to the quadratic (*p*-value < 0.0001, R² = 0.97) and that the effect of the MTBE concentration is greater than the others. The highest removal efficiency was taken in an initial concentration of 37.5 mg/L MTBE, 1.58 mg/L Fe₂O₃/MgO, pH 5, and a reaction time of 21.41 min without any As. The removal efficiency was negatively correlated with the initial MTBE concentration and pH, but it was positively associated with the Fe₂O₃/MgO dosage and reaction time. Finally, the presence of arsenic decreased the removal efficiency remarkably (90.90% As = 0.25 µg/L and 61% As = 500 µg/L). Consequently, MTBE was removed by the photocatalytic process caused by Fe₂O₃/MgO, but the presence of arsenic was introduced as a limiting factor. Therefore, pretreatment for the removal of arsenic and more details of this interference effect are suggested.

Keywords: MTBE; arsenic; Fe₂O₃/MgO catalyst; AOP; modeling; optimization



Citation: Mehdizadeh, A.; Derakhshan, Z.; Abbasi, F.; Samaei, M.R.; Baghapour, M.A.; Hoseini, M.; Lima, E.C.; Bilal, M. The Effect of Arsenic on the Photocatalytic Removal of Methyl Tet Butyl Ether (MTBE) Using Fe₂O₃/MgO Catalyst, Modeling, and Process Optimization. *Catalysts* **2022**, *12*, 927. <https://doi.org/10.3390/catal12080927>

Academic Editor: John Vakros

Received: 29 June 2022

Accepted: 18 August 2022

Published: 22 August 2022

Publisher's Note: MDPI stays neutral with regard to jurisdictional claims in published maps and institutional affiliations.



Copyright: © 2022 by the authors. Licensee MDPI, Basel, Switzerland. This article is an open access article distributed under the terms and conditions of the Creative Commons Attribution (CC BY) license (<https://creativecommons.org/licenses/by/4.0/>).

1. Introduction

Water pollution due to petroleum compounds such as MTBE is one of the main problems in water resources [1,2]. MTBE is classified as an oxygenated compound added to gasoline to restore combustion [3]. MTBE has expanded as an octane booster and anti-knocking agent in the past two decades due to its low cost and easy usage, transition, and distribution. MTBE, (CH₃)₃COCH₃, is a volatile, colorless, and flammable liquid, and it is soluble in water (48 g/L at 25 °C). However, it causes environmental and health effects (IARC), such as nervous system reactions, dizziness, distraction, nausea, and forgetfulness [4,5]. Moreover, it has a low-threshold taste and odor (40 and 15 µg/L, respectively) [6]. The maximum contaminant level of MTBE in drinking water has been determined to be

20–40 µg/L by the USEPA. MTBE enters groundwater in various ways, such as leakage from road accidents, underground storage tanks (USTs), and pipelines [7,8].

The effective removal of MTBE from water is essential. Many attempts have been made over the past decades to eliminate MTBE from groundwater. However, MTBE removal using conventional water treatment processes is difficult due to its high solubility, low tendency to the soil, resistance to degradation, the presence of ether bands, and its resistant carbon chain [9–13]. The most commonly used processes for MTBE removal are adsorption using activated carbon, air stripping, and advanced oxidation processes (AOPs). According to previous studies, AOPs, especially photocatalytic oxidation, are the most effective for MTBE decomposition [14–18]. AOPs can remove MTBE effectively, but their efficiency depends on the water-quality characteristics and the level of other contaminants, such as metals [19–21], because the oxidation of metals during AOPs might decrease the efficiency of MTBE removal.

Arsenic is a highly toxic metalloid, and its presence in water is a global problem. Elevated concentrations of arsenic have been detected in some parts of the world, including Bangladesh; India; some South American countries, such as Argentina; and some areas of Kurdistan and Hashtrud in Iran [22]. Arsenic leaches into water from natural and anthropogenic sources, including biological activities, volcanic releases, and human activities, such as the use of pesticides and minerals. Therefore, investigating the removal efficiency of organic matter in arsenic-contaminated water is essential. As(III), oxidized to As(V) during photocatalytic oxidation [23], can be considered a competitor for the removal of organic matter (such as MTBE). One suggested solution is a combination process with a high oxidation capacity, such as the photocatalytic process. The initial energy obtained from the photo resource and the activation energy is decreased using catalysts in the photocatalytic process.

In this study, Fe₂O₃/MgO was used as a catalyst because it is a porous structure with a high capacity for adsorbing organic matter [24,25] and generating free radicals [26]. Moreover, its band gap is 5.4–5.45 eV, so the electron in the band layer excites the current layer [24]. Therefore, its photocatalytic effect is performed when it is exposed to UV radiation. In other words, MgO doped with a metal oxide improves photocatalytic activity [27,28]. So, the removal efficiency of organic dye using Fe₂O₃-doped MgO is estimated to be above 92% after five regenerations [29] therefore, the combination of MgO and Fe₂O₃ can improve the removal efficiency of organic matter, such as MTBE, which is used for the first time in this study. In an earlier study, the photocatalytic process was used for MTBE removal [30], but there was less attention paid to the effect of metal, especially arsenic, on the MTBE's removal efficiency. For example, Zhang et al. (2018) reported that nickel decreased the adsorption capacity of MTBE using ZSM-5 zeolite [6]. However, for the first time, this study focuses on the decreasing trend in the photocatalytic oxidation of MTBE using Fe₂O₃/MgO due to arsenic.

Arsenic, as a semimetal, can participate in electron-hole processes in aqueous solutions so that it turns into arsenic with an oxidation number of five during the redox reaction. Since the photocatalytic process is a suitable method for mineralizing organic compounds such as MTBE, the released radicals ultimately cause water treatment. Therefore, the paths for both arsenic deposition and photocatalytic reactions are the same, which greatly increases the possibility of interference. Numerous studies have examined the effect of some metals on interference in the photocatalytic process, including the formation, recombination, and formation rate of radicals. However, these effects have been less investigated when considering semimetals, especially arsenic. Due to the existence of a variety of arsenic concentrations in the water resources of Iran and other regions of the world; the high potential of semiconductors for active participation in electron transfer processes; and the strong tendency for arsenic to change its oxidation number and phase from soluble to insoluble forms in aqueous solutions exposed to the photocatalytic process, the present study aims to model and determine the interference effect on a laboratory scale for the first time in order to consider the type and amount of interference effect in the treatment

of water resources using the photocatalytic process on a real scale and optimize the parameters accordingly.

Arsenic is a toxic metalloid detected in some water supplies, such as in Iran. Concerning the oxidation potential of arsenic in an aqueous solution, it is expected that its interference in the photocatalytic removal of organic matter includes MTBE. Regarding the significant concern about MTBE, the high concentrations of arsenic that have been reported in some areas of Iran, and its interference effect on the mineralization and degradation of MTBE, as well as the lack of documents, imply the effect of metals on the removal efficiency of organic matter. Therefore, this study aims to investigate the effect of arsenic on the photocatalytic oxidation process of MTBE using $\text{Fe}_2\text{O}_3/\text{MgO}$ as a catalyst. Moreover, the interactions between the effective factors and the optimization of the process were determined by the response surface methodology (RSM) method.

2. Results

2.1. Specification of the Catalyst

2.1.1. SEM–EDX Analysis

SEM determined the microstructure and morphology of the catalyst, and its images are shown in Figure 1.

The synthesized catalyst has a uniform and aggregated structure, making separation from the liquid effluent easier after the photocatalytic process [31]. In addition, it has good dispersion, and the sample has a diameter of approximately 2 μm . In Figure 1b, the elements' quantitative levels in the nanocatalyst were determined using EDX, confirming the presence of the elements MgO (45.06%) and Fe_2O_3 (33.06%) in the synthesized catalyst.

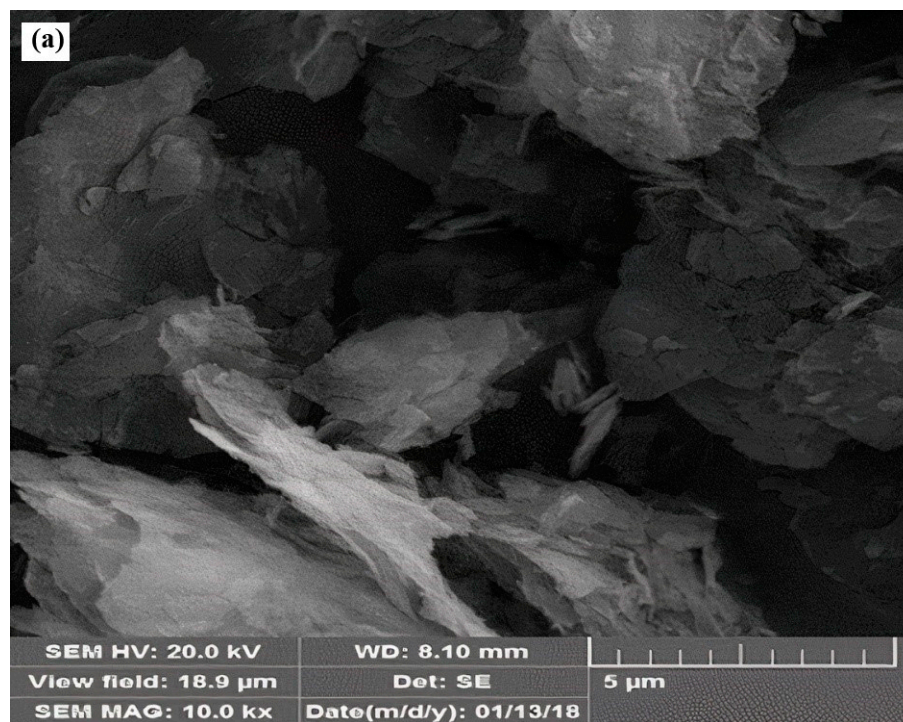


Figure 1. Cont.

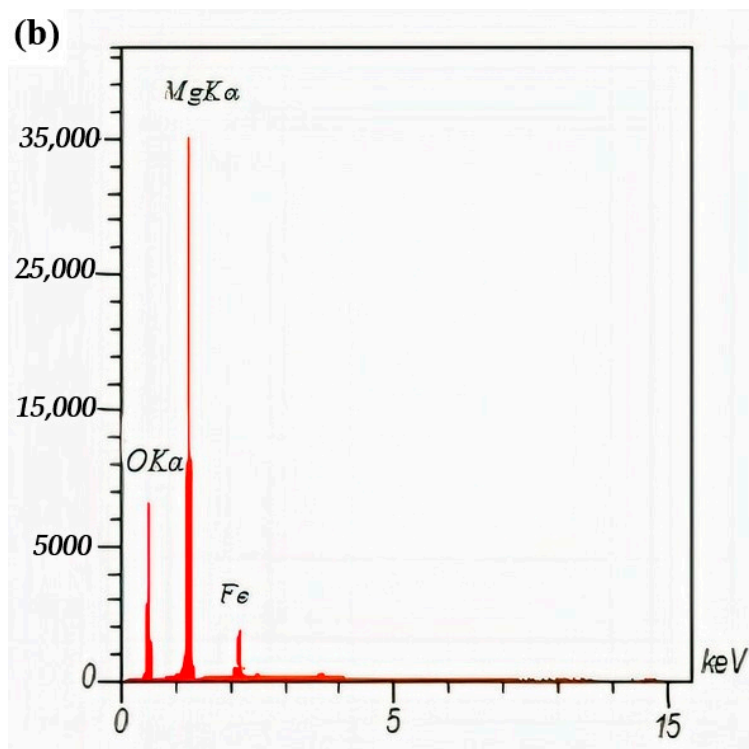


Figure 1. SEM (a) and EDX (b) images for the nanocatalyst.

2.1.2. XRD Analysis

The XRD analysis ($10\text{--}80^\circ 2\theta$) of the nanocatalyst is shown in Figure A1. The average crystal size of the sample was calculated using the Scherrer equation: ($d = K\lambda / (\beta \cos \theta)$). The strong and sharp peaks in Figure A1 suggest that the nanocatalyst has a crystalline structure. The values for Fe_2O_3 and MgO were 91.1 and 27.9 nm, respectively. As shown in the figure, the diffraction peaks of both Fe_2O_3 and MgO could be observed. The blue peaks are associated with Fe_2O_3 , and the red peaks are related to MgO . This nanocatalyst had two peaks at 33.06° and 36.5° that can be associated with Fe_2O_3 and MgO , respectively. According to Figure A1, the peaks related to Fe_2O_3 are wholly covered over by MgO 's peaks, indicating the high precision of the sol-gel process.

2.2. Photocatalytic Removal of MTBE

The interactions between independent and dependent variables while removing MTBE were investigated in DE7.

The effect of the $\text{Fe}_2\text{O}_3/\text{MgO}$ nanocatalyst dosage, pH, and initial MTBE concentrations on the photocatalytic removal efficiency and optimization of these variables was investigated by Factorial Experimental Design. The MTBE's lowest, highest, and average removal efficiencies were 61%, 90.90% and 73%, respectively. The ANOVA results for the proposed model for the photocatalytic removal of MTBE based on the experiment's results and the effect of the parameters are presented in Table 1. The F-value and *p*-value for MTBE were 835.92 and >0.0001 , respectively. Thus, the *p*-value of the investigated parameters ($p \leq 0.05$) shows that the concentration of MTBE and the concentration of catalyst are effective parameters for the photocatalytic oxidation of MTBE (Table 1).

In the model, the F-value also shows that the defined parameters in the models have significant effects, and the effect of the initial MTBE concentration was more pronounced than other parameters. However, only a 0.01% chance of the occurrence of the F-value was due to noise. The effects of the significant parameters based on the suggested model are presented in Equation (1) and Figure A2, which are used for predicting the photocatalytic oxidation values of MTBE.

$$\text{MTBE} = 18.70 + 11.32^{\text{a}} - 0.89\text{C} + 1.03\text{BC} - 1.43\text{DE} - 1.38\text{B}^2 \quad (1)$$

The MTBE residual was increased based on the model equation, increasing the MTBE (A) concentration and decreasing the catalyst (C). Furthermore, the factors for interactions, such as concentration of arsenic \times concentration of catalyst, which had a positive effect and the effect of pH \times time, which had a negative effect on the response, and the response affected the quadratic of the arsenic concentration. Based on any of the coefficients, the effect of the catalyst was higher than other parameters.

Table 1. ANOVA results for the Response Surface Quadratic Model (MTBE).

Source	Sum of Squares	df	Mean Squares	F-Value	p-Value
Model	5624.73				
A—MTBE	5122.75	20	281.24	45.84	
B—Arsenic	15.89	1	5122.75	834.92	<0.0001
C—Catalyst	31.60	1	15.89	2.59	<0.0001
D—pH	5.23	1	31.60	5.15	0.1184
E—Time	9.19	1	5.23	0.85	0.0309
AB	6.53	1	9.19	1.50	0.3633
AC	9.26	1	6.53	1.06	0.2309
AD	0.043	1	9.26	1.51	0.3109
AE	8.09	1	0.043	6.972	0.2292
BC	33.97	1	8.09	1.32	0.9340
BD	4.34	1	33.97	5.54	0.2602
BE	0.10	1	4.34	0.71	0.0256
CD	23.27	1	0.10	0.016	0.4070
CE	8.85	1	23.27	3.79	0.8992
DE	65.24	1	8.85	1.44	0.0612
A2	14.39	1	65.24	10.63	0.2394
B2	60.78	1	14.39	2.35	0.0028
C2	183.26	1	60.78	9.91	0.1365
D2	21.88	1	183.26	29.87	0.0038
E2	0.078	1	21.88	3.57	<0.0001
Residual	177.93	1	0.078	0.013	0.0690
Lack of Fit	159.44	29	6.14		0.9111
Pure Error	18.49	22	7.25	2.74	
Cor Total	5802.67	7	2.64		0.0868
		49			

Moreover, the perturbation plot of independent variables on the photocatalytic oxidation of MTBE is shown in Figure A2.

According to Figure A2, the most influential factor was MTBE concentration. Moreover, the effect of arsenic concentration on the MTBE photocatalytic process was insignificant.

The proportion of predicted values of the photocatalytic oxidation efficiency of As(III) in the model and the actual values obtained from the experiments are shown in Figure 2.

The determination coefficient for the actual and predicted values of residual MTBE was acceptable ($R^2 = 0.9693$). The difference between the adjusted determination coefficient ($\text{Adj } R^2$) and the predicted determination coefficient ($\text{Pred } R^2$) should not be more than 0.2 [32]. Based on the results, this difference was 0.0498, indicating the model's adequacy. Furthermore, R^2 0.97 for MTBE shows that the model can explain about 97 data variations. The calculated lack of fit in these models is 2.74, which is not significant; therefore, the disordered data do not affect the model.

The Simultaneous Effect of the Concentration of $\text{Fe}_2\text{O}_3/\text{MgO}$ and Initial MTBE

The efficiency of MTBE removal at various initial concentrations of MTBE and the $\text{Fe}_2\text{O}_3/\text{MgO}$ catalyst is shown in Figure 3.

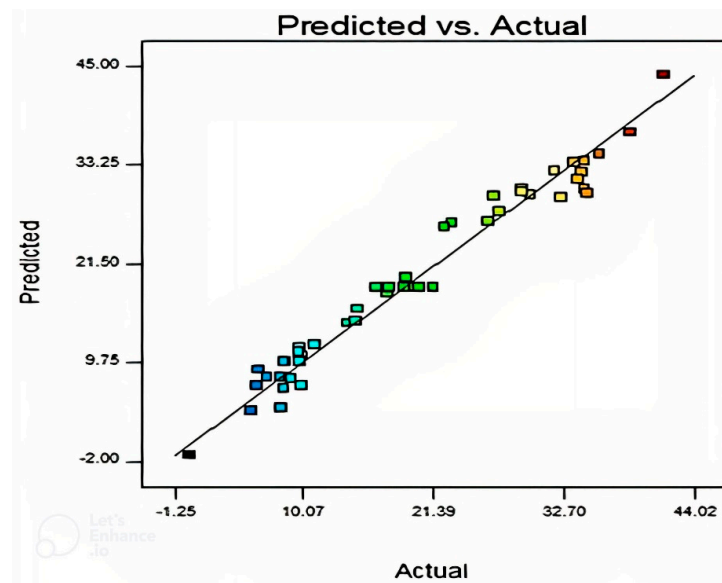


Figure 2. Predicted versus actual experimental results for residual MTBE.

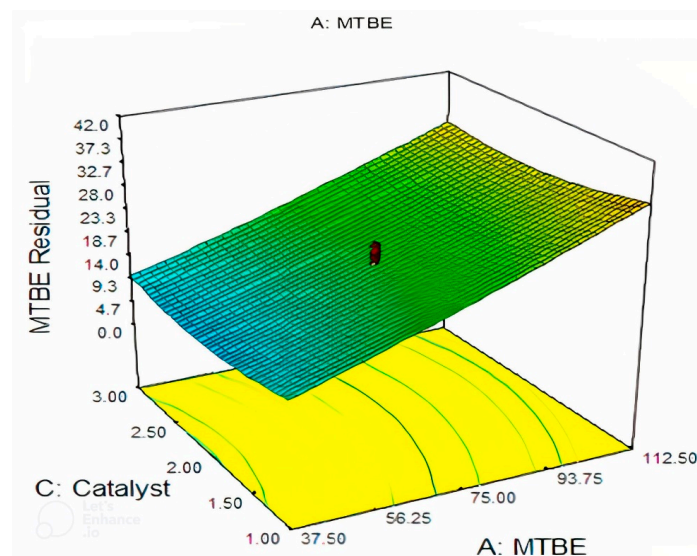
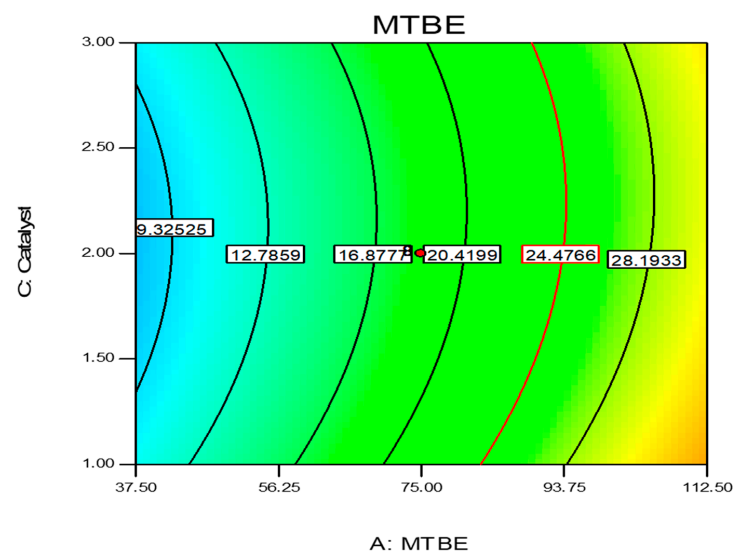


Figure 3. Contour and 3D Plots of the interactive effect of catalyst dosage (g/L) and MTBE (mg/L).

According to Figure 3, 1–2.5 g/L of catalyst can slightly increase MTBE's removal efficiency, while a catalyst concentration of more than 4 g/L had a negative effect. This is because the number of photons and adsorbed molecules in a high catalyst level also increases. This reaction increased the particle density in the brightness range and the amount of free radicals that improved the degradation of MTBE. However, a further increase in the catalyst dosage caused the reduction in active sites on the surface of Fe₂O₃/MgO. Therefore, the removal efficiency of MTBE was decreased [33,34]. Concerning this result, the best concentration of nanoparticles was 1.54 g/L, but the higher concentrations increased costs.

3. Materials and Methods

3.1. Materials

All the analytical-grade chemical materials, including MTBE, sodium arsenite (NaAsO₂), magnesium oxide (MgO), hematite (Fe₂O₃), sodium hydroxide (NaOH), hydrochloric acid (HCL), citric acid (C₆H₈O₇), acetone (C₃H₆O), hexane (C₆H₁₄), and ethanol (C₂H₆O), were purchased from Sigma Aldrich Company (St. Louis, MI, USA). NaOH and HCl were used for adjusting the pH. The double-distilled water (18 MΩ cm) was applied to prepare the solutions. A UV lamp (11W) was used for the light supply. A powder X-ray diffractometer (XRD) (Philips PW 1800, Round Rock, TX, USA) was used to determine the gel structure. Scanning electron microscopy (SEM) (Carl-Zeiss-Promenade, Jena, Germany) measurement (HV: 20.0 kV) was used to envisage the nanoparticles' surface morphology.

3.2. Preparation of the Catalyst

In a typical process, highly active MgO nanoparticles were prepared via a simple sol–gel method. First, the MgO nanoparticles were dissolved in ethanol at 60 °C for 5 h, and citric acid was added slowly to form the gelling solution by stirring. When the solution was completely dispersed, the compound was concentrated at 65 °C to form a wet gel. The wet gel was then dried at 110 °C for 12 h. Finally, the above-obtained product was calcinated at 550 °C with a heating rate of 4 °C min^{−1} for 4 h. The Fe₂O₃ solution was synthesized by the sol–gel method. This solution was joined to make the final coating with the MgO gel to obtain the final product of Fe₂O₃/MgO [30].

3.3. Stability and Reusability of the Catalyst

To examine the stability of the catalyst, 1 g/L of the catalyst was placed in the simulated conditions of the experiments, and then, the concentrations of iron and magnesium remaining in the solution were measured after 0–50 min as described in Table 2.

Table 2. Concentration of iron and magnesium remaining in the solution after 0–50 min.

Time (min)	0	10	20	30	40	50
Mg (mg/L)	0	2.02	3	3.9	4.3	6.1
Fe (mg/L)	0	5.7	12.6	17.2	21.4	26.3

The leakage rate of both magnesium and iron in the aqueous solution was less than 5% during the laboratory conditions, which was statistically confirmed.

After performing the photocatalytic process, the studied reactor was placed in the magnetic field to investigate the secondary application of the catalyst in laboratory conditions during the study period, the efficiency of which was favorable. After drying the catalyst at 70 °C, the collected catalyst was weighed on a scale, and the weight difference was estimated to be less than 15%. Moreover, the catalyst was photographed after the photocatalytic process, which did not differ significantly from the initial images. Thus, it can be said that the MTBE mineralization and removal operations were carried out under suitable conditions.

3.4. Sample Preparation

This study used a high-purity MTBE solution (99.9%). An arsenite stock solution (1000 mg/L) was prepared by dissolving potassium arsenite (KAsO₂) in distilled water (acid-distilled twice) with HCl (with a final concentration of 2.5%). The samples were stored in a refrigerator at 4 °C after preparation. NaOH and HCL were used to adjust the reaction mixture's pH.

3.5. Chemical Reactor and Optimization

The photocatalytic removal of MTBE was carried out in a laboratory-scale batch slurry reactor. The reactor comprised transparent Plexiglas with dimensions (length, width, and height) of 20 × 10 × 14 cm and 1 L effective volume. A UV lamp (11 W) was submerged in the solution to provide UV radiation for the reactor. First, the reactor was tightly closed and stirred completely. Then, the reactor was fixed and made in the two-seated form. The temperature of the reactor was controlled at 25–30 °C. Then, the solution was centrifuged (at 4000 rpm for 30 min) to separate the nanocatalyst.

The design of the experiments was performed based on a partial factorial method. Table 3 lists the values and variables used in the design of the experiments.

Table 3. Natural and coded levels of independent variables based on the central composite design.

Independent Variable	Symbol	Coded Level				
		−2	−1	0	1	2
				Natural Level		
MTBE (mg/L)	A	0	37.5	75	112.5	150
Arsenic (mg/L)	B	0	0.25	0.5	0.75	1
Catalyst (g/L)	C	0	1	2	3	4
pH	D	3	5	7	9	11
Time (min)	E	10	20	30	40	50

The values of the natural and coded independent variables were designed based on the central composite design (CCD). The order of each experiment was selected randomly by Design Expert 7 (DE7) software based on past studies and observed values in Iran's groundwaters. To more closely look at the effect of each variable on the process, one of the values of MTBE, the catalyst or arsenic, is considered zero in the DE7. Finally, 50 experiments were designed as Factorial Designs.

3.6. MTBE Extraction Method

MTBE was extracted using the dispersive liquid–liquid microextraction (DLLME) method. DLLME is a simple, fast, and sensitive method for extracting organic compounds from aqueous solutions [35]. First, 10 mL of the sample was added to a glass tube with a conical bottom centrifuge tube. The acetonitrile (1 mL) and hexane (0.2 mL) were used as dispersing and extraction solutions, respectively. Next, the mixture solution was centrifuged at 5000 rpm for 2 min. After this stage, hexane droplets were separated, removed with a 10 µL Hamilton syringe, and injected into the GC.

3.7. Data Analysis

Data analysis was performed using the RSREG method in DE7. The regression coefficients of the empirical data were generalized as a quadratic polynomial model [36]. This model is as follows in Equation (2):

$$Y = \beta_0 + \sum_{i=1}^3 \beta_i X_i + \sum_{i=1}^3 \beta_{ii} X_i^2 + \sum_{i<j=1}^3 \beta_{ij} X_i X_j \quad (2)$$

Y = the amount of MTBE, β_0 = interactive regression coefficients, β_i = linear regression coefficients, β_{ii} = quadratic regression coefficients, β_{ij} = interactive regression coefficients, and X_i and X_j = dependent variables

ANOVA was used to determine the significance of the model and independent variables and determine the values of R^2 , R^2_{adjusted} , and $R^2_{\text{predicted}}$. The p -value and lack of fit in the variance analysis table, the normal curves, and the predicted values versus the real values were used to check the model's desirability and data. The statistically significant level of the p -value was 0.05 [37]. The lack of fit value should not be meaningful (meaning any distorted data in the model). The contours and three-dimensional charts were plotted to analyze the removal rate of MTBE and the interactions of independent variables. Finally, the RSM-obtained optimal conditions for removing MTBE and arsenic were obtained using predicted equations.

4. Conclusions

Although the photocatalytic process is a suitable method for treating MTBE in an aqueous solution, the presence of some contaminants can be a limiting factor for efficient removal. Arsenic is a metalloid that oxidizes during the photocatalytic process and competes with MTBE for oxidation. In general, it can be concluded that the method used in this study is more suitable for lower concentrations of MTBE. Although less attention was paid to the effect of As on water treatment, this study showed that the presence of arsenic in water could limit the efficiency of removal of MTBE. Since there is arsenic in some water resources and MTBE leaching, pretreatment for the removal of arsenic is essential. The photocatalytic process is more cost-effective than other methods used to remove organic compounds, such as air stripping, GAC, incineration, and ozonation. This process generally destroys organic pollutants at an ambient temperature and pressure without any need for direct oxygen injection. However, this treatment method is applicable in conditions that are optimal in economic, environmental, and operational terms. The presence of some inhibitory and disruptive factors, such as arsenic, in the water environment could reduce the process efficiency. Therefore, it could be argued that arsenic separation and removal before the photocatalytic process is one of the best options for decreasing this inhibitory effect, which reduces downstream treatment costs.

In this study, the inhibitory effect of arsenic on the photocatalytic oxidation process of MTBE using $\text{Fe}_2\text{O}_3/\text{MgO}$ was investigated. The $\text{Fe}_2\text{O}_3/\text{MgO}$ nanocatalyst was successfully synthesized based on the SEM, EDX, and XRD analyses. The results showed that MTBE was removed successfully by photocatalytic oxidation and the best model was the quadratic model ($p < 0.0001$, $F = 45.84$, $R^2 = 0.9693$, $R^2_{\text{adjusted}} = 0.9482$, and $R^2_{\text{predicted}} = 0.8984$). According to the quadratic model and ANOVA analysis, the most effective factors were the initial concentration of MTBE and the catalyst dosage. The process optimization expressed that the efficiency of the MTBE oxidation process was improved by increasing both the catalyst dosage and time and decreasing MTBE and the pH. The predicted and experimental removal efficiencies were 90.90% and 88.73%, respectively, under the optimal conditions (initial concentration of MTBE = 37.5 mg/L, pH = 5, Catalyst = 1.54 g/L, and Time = 21.41 min). Although the process successfully removed MTBE, arsenic was introduced as an inhibitor factor. So, the highest inhibitory effect related to the initial arsenic is 0.5 mg/L. Concerning these results, the pretreatment of arsenic from water resources and more details about the inhibitory effect of arsenic on the photocatalytic removal of MTBE, such as the formation of hole-electrons, is essential. Moreover, further studies are suggested to determine the effect of other heavy metals and metalloids on organic matter removal efficiency.

Author Contributions: Conceptualization, A.M. and M.R.S.; methodology, F.A.; software, M.A.B. and A.M.; validation, M.H.; investigation, Z.D.; resources, E.C.L.; writing—review and editing, M.B. and E.C.L. All authors have read and agreed to the published version of the manuscript.

Funding: This research received no external funding.

Data Availability Statement: The data presented in this study are available on request from the corresponding author.

Acknowledgments: This article was extracted from a thesis written by Akbar Mehdizadeh (proposal No. 14140), which Shiraz University of Medical Sciences financially supported.

Conflicts of Interest: The authors declare no conflict of interest.

Appendix A

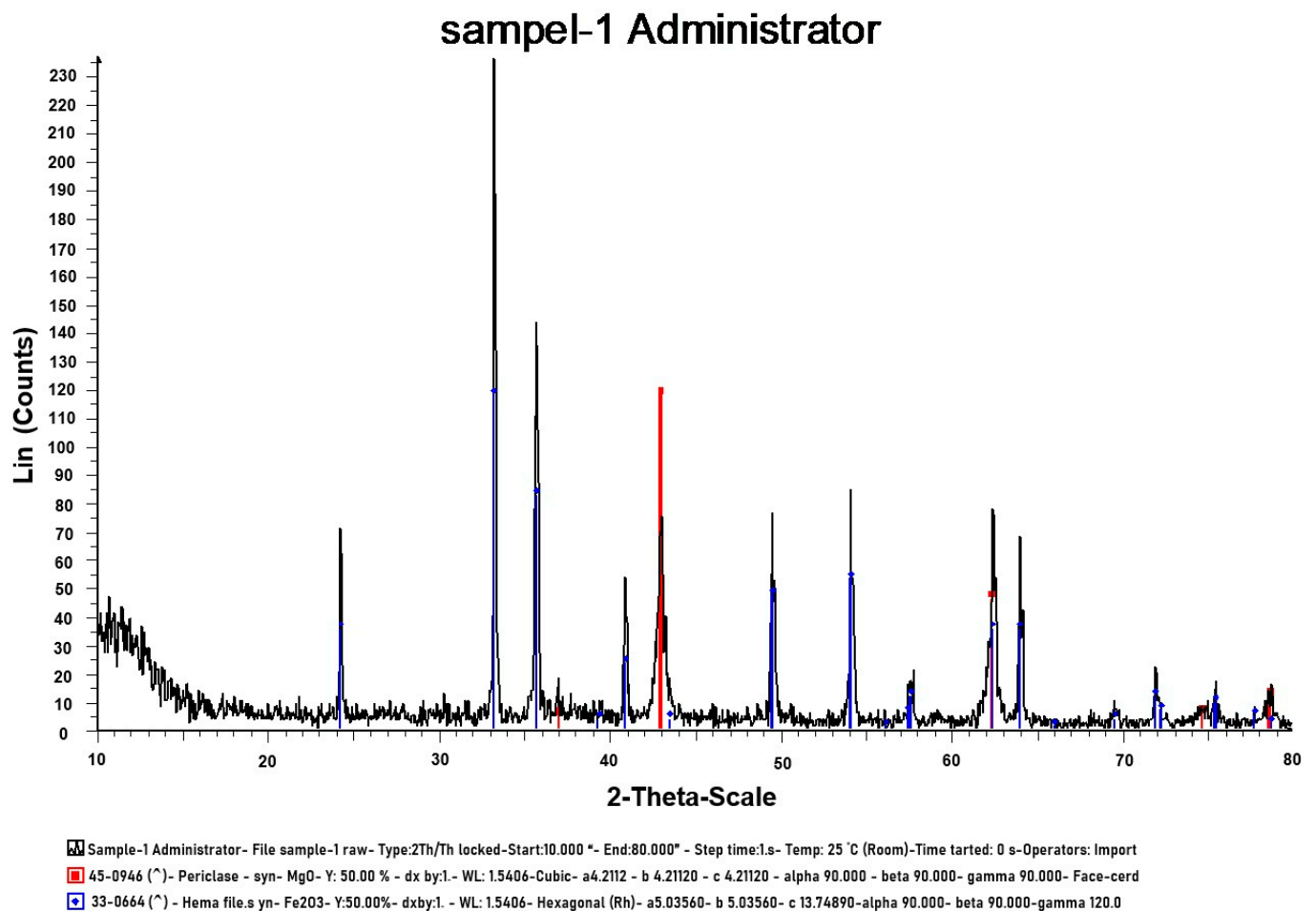


Figure A1. XRD patterns of Fe_2O_3 and MgO .

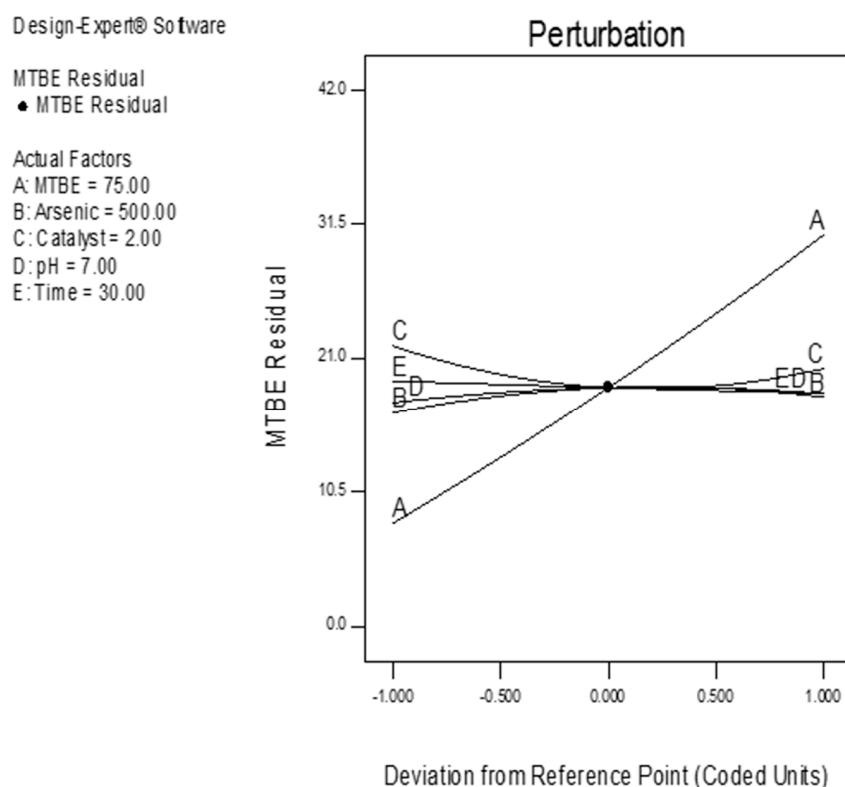


Figure A2. The perturbation Plot of independent variables in the photocatalytic oxidation of MTBE.

References

- Jorfi, S.; Samaei, M.R.; Soltani, R.D.C.; Talaiekhosani, A.; Ahmadi, M.; Barzegar, G.; Reshadatian, N.; Mehrabi, N. Enhancement of the bioremediation of pyrene-contaminated soils using a hematite nanoparticle-based modified Fenton oxidation in a sequenced approach. *Soil Sediment Contam. Int. J.* **2017**, *26*, 141–156. [[CrossRef](#)]
- Ekinci, E.K. Mesoporous magnesia sorbent for removal of organic contaminant methyl tert -butyl ether (MTBE) from water. *Sep. Sci. Technol.* **2022**, *57*, 843–853. [[CrossRef](#)]
- Shamim, M.; Aalam, C.S.; Manivannan, D.; Kumar, S. Characterization of Gasoline Engine Using MTBE and DIE Additives. *Int. Res. J. Eng. Technol.* **2017**, *4*, 191–199.
- International Agency for Research on Cancer. *IARC Monographs on the Evaluation of Carcinogenic Risks to Humans*; IARC: Lyon, France, 1994; pp. 389–433.
- Mahmoodsaleh, F.; Ardakani, M.R. Methyl tertiary butyl ether biodegradation by the bacterial consortium isolated from petrochemical wastewater and contaminated soils of Imam Khomeini Port Petrochemical Company (Iran). *Bioremed. J.* **2021**, *26*, 127–137. [[CrossRef](#)]
- Zhang, Y.; Jin, F.; Shen, Z.; Lynch, R.; Al-Tabbaa, A. Kinetic and equilibrium modelling of MTBE (methyl tert-butyl ether) adsorption on ZSM-5 zeolite: Batch and column studies. *J. Hazard. Mater.* **2018**, *347*, 461–469. [[CrossRef](#)]
- Samaei, M.R.; Maleknia, H.; Azhdarpoor, A. A comparative study of removal of methyl tertiary-butyl ether (MTBE) from aquatic environments through advanced oxidation methods of $H_2O_2/nZVI$, $H_2O_2/nZVI/ultrasound$, and $H_2O_2/nZVI/UV$. *Desalination Water Treat.* **2016**, *57*, 21417–21427. [[CrossRef](#)]
- Beryani, A.; Pardakhti, A.; Ardestani, M.; Zahed, M.A. Benzene and MTBE removal by Fenton's process using stabilized Nano Zero-Valent Iron particles. *J. Appl. Res. Water Wastewater* **2017**, *4*, 343–348.
- Lindsey, D.; Ayotte, J.D.; Jurgens, B.C.; Desimone, L.A. Using groundwater age distributions to understand changes in methyl tert-butyl ether (MtBE) concentrations in ambient groundwater, northeastern United States. *Sci. Total Environ.* **2017**, *579*, 579–587. [[CrossRef](#)]
- Khademi, S.M.S.; Tabrizchi, M.; Telgheder, U.; Valadbeigi, Y.; Ilbeigi, V. Determination of MTBE in drinking water using corona discharge ion mobility spectrometry. *Int. J. Ion Mobil. Spectrom.* **2017**, *20*, 15–21. [[CrossRef](#)]
- Abbas, A.; Sallam, A.S.; Usman, A.R.A.; Al-Wabel, M.I. Organoclay-based nanoparticles from montmorillonite and natural clay deposits: Synthesis, characteristics, and application for MTBE removal. *Appl. Clay Sci.* **2017**, *142*, 21–29. [[CrossRef](#)]
- Pirsaheb, M.; Dargahi, A.; Khamutian, R.; Asadi, F.; Atafar, Z. A survey of methyl tertiary butyl ether concentration in water resources and its control procedures. *J. Maz. Univ. Med. Sci.* **2014**, *24*, 119–128.
- Iraji, G.; Givianrad, M.H.; Tehrani, M.S. Highly efficient degradation of MTBE by $\gamma-Al_2O_3/NiO/TiO_2$ core-shell nanocomposite under visible light irradiation. *Int. J. New Chem.* **2021**, *8*, 222–228. [[CrossRef](#)]

14. Andreozzi, R.; Caprio, V.; Insola, A.; Marotta, R. Advanced oxidation processes (AOP) for water purification and recovery. *Catal. Today* **1999**, *53*, 51–59. [[CrossRef](#)]
15. Tsimas, E.S.; Tyrovolas, K.; Xekoukoulotakis, N.P.; Nikolaidis, N.P.; Diamadopoulos, E.; Mantzavinos, D. Simultaneous photocatalytic oxidation of As (III) and humic acid in aqueous TiO₂ suspensions. *J. Hazard. Mater.* **2009**, *169*, 376–385. [[CrossRef](#)]
16. López-Muñoz, M.J.; Arencibia, A.; Segura, Y.; Raez, J.M. Removal of As (III) from aqueous solutions through simultaneous photocatalytic oxidation and adsorption by TiO₂ and zero-valent iron. *Catal. Today* **2017**, *280*, 149–154. [[CrossRef](#)]
17. Barkoula, N.-M.; Alcock, B.; Cabrera, N.O.; Peijs, T. Fatigue properties of highly oriented polypropylene tapes and all-polypropylene composites. *Polym. Polym. Compos.* **2008**, *16*, 101–113. [[CrossRef](#)]
18. Pal, D.; Lavania, R.; Srivastava, P.; Singh, P.; Srivastava, K.; Madhav, S.; Mishra, P. Photocatalytic degradation of methyl tertiary butyl ether from wastewater using CuO/CeO₂ composite nanofiber catalyst. *J. Environ. Chem. Eng.* **2018**, *6*, 2577–2587. [[CrossRef](#)]
19. Tawabini, B.; Makkawi, M. Remediation of MTBE-contaminated groundwater by integrated circulation wells and advanced oxidation technologies. *Water Sci. Technol. Water Supply* **2018**, *18*, 399–407. [[CrossRef](#)]
20. Smedley, P.L.; Kinniburgh, D.G. Source and behaviour of arsenic in natural waters. In *United Nations Synthesis Report on Arsenic in Drinking Water*; World Health Organization: Geneva, Switzerland, 2001; pp. 1–61.
21. Ghayurdoost, F.; Assadi, A.; Mehrasbi, M.R. Removal of MTBE From Groundwater Using A PRB of ZVI/Sand Mixtures: Role of Nitrate And Hardness. *Res. Square* **2021**. [[CrossRef](#)]
22. Azhdarpoor; Nikmanesh, R.; Samaei, M.R. Removal of arsenic from aqueous solutions using waste iron columns inoculated with iron bacteria. *Environ. Technol* **2015**, *36*, 2525–2531. [[CrossRef](#)]
23. Eslami, H.; Ehrampoush, M.H.; Esmaeili, A.; Ebrahimi, A.A.; Salmani, M.H.; Ghaneian, M.T.; Falahzadeh, H. Efficient photocatalytic oxidation of arsenite from contaminated water by Fe₂O₃-Mn₂O₃ nanocomposite under UVA radiation and process optimization with experimental design. *Chemosphere* **2018**, *207*, 303–312. [[CrossRef](#)]
24. Balakrishnan, J.; Sreeshma, D.; Siddesh, B.M.; Jagtap, A.; Abhale, A.; Rao, K.K. Ternary alloyed HgCdTe nanocrystals for short-wave and mid-wave infrared region optoelectronic applications. *Nano Express* **2020**, *1*, 020015. [[CrossRef](#)]
25. Beltrán, D.E.; Uddin, A.; Xu, X.; Dunsmore, L.; Ding, S.; Xu, H.; Zhang, H.; Liu, S.; Wu, G.; Litster, S. Elucidation of Performance Recovery for Fe-Based Catalyst Cathodes in Fuel Cells. *Adv. Energy Sustain. Res.* **2021**, *2*, 2100123. [[CrossRef](#)]
26. Chan, S.H.S.; Wu, T.Y.; Juan, J.C.; Teh, C.Y. Recent developments of metal oxide semiconductors as photocatalysts in advanced oxidation processes (AOPs) for treatment of dye waste-water. *J. Chem. Technol. Biotechnol.* **2011**, *86*, 1130–1158. [[CrossRef](#)]
27. Sierra-Fernandez, A.; De la Rosa-García, S.C.; Yañez-Macías, R.; Guerrero-Sanchez, C.; Gomez-Villalba, L.S.; Gómez-Cornelio, S.; Rabanal, M.E.; Schubert, U.S.; Fort, R.; Quintana, P. Sol-gel synthesis of Mg(OH)₂ and Ca(OH)₂ nanoparticles: A comparative study of their antifungal activity in partially quaternized p(DMAEMA) nanocomposite films. *J. Sol-Gel Sci. Technol.* **2019**, *89*, 310–321. [[CrossRef](#)]
28. Popov, A.; Shirmane, L.; Pankratov, V.; Lushchik, A.; Kotlov, A.; Serga, V.; Kulikova, L.; Chikvaidze, G.; Zimmermann, J. Comparative study of the luminescence properties of macro- and nanocrystalline MgO using synchrotron radiation. *Nucl. Instrum. Methods Phys. Res. Sect. B Beam Interact. Mater. Atoms* **2013**, *310*, 23–26. [[CrossRef](#)]
29. Zheng, S.; Zhou, Q.; Chen, C.; Yang, F.; Cai, Z.; Li, D.; Geng, Q.; Feng, Y.; Wang, H. Role of extracellular polymeric substances on the behavior and toxicity of silver nanoparticles and ions to green algae *Chlorella vulgaris*. *Sci. Total Environ.* **2019**, *660*, 1182–1190. [[CrossRef](#)] [[PubMed](#)]
30. Aghamohammadi, S.; Haghighi, M.; Karimipour, S. A comparative synthesis and physicochemical characterizations of Ni/Al₂O₃-MgO nanocatalyst via sequential impregnation and sol-gel methods used for CO₂ reforming of methane. *J. Nanosci. Nanotechnol.* **2013**, *13*, 4872–4882. [[CrossRef](#)]
31. Berijani, S.; Assadi, Y.; Anbia, M.; Hosseini, M.-R.M.; Aghaee, E. Dispersive liquid-liquid microextraction combined with gas chromatography-flame photometric detection: A very simple, rapid and sensitive method for the determination of organophosphorus pesticides in water. *J. Chromatogr. A* **2006**, *1123*, 1–9. [[CrossRef](#)]
32. Khuri, I. *Response Surface Methodology and Related Topics*; World Scientific: Singapore, 2006.
33. Salmani, M.H.; Mokhtari, M.; Raeisi, Z.; Ehrampoush, M.H.; Sadeghian, H.A. Evaluation of removal efficiency of residual diclofenac in aqueous solution by nanocomposite tungsten-carbon using design of experiment. *Water Sci. Technol.* **2017**, *76*, 1466–1473. [[CrossRef](#)]
34. Habibi, M.H.; Mosavi, V. Synthesis and characterization of Fe₂O₃/Mn₂O₃/FeMn₂O₄ nanocomposite alloy coated glass for photocatalytic degradation of Reactive Blue 222. *J. Mater. Sci. Mater. Electron.* **2017**, *28*, 11078–11083. [[CrossRef](#)]
35. Akyol, A.; Can, O.T.; Demirbas, E.; Kobya, M. A comparative study of electrocoagulation and electro-Fenton for treatment of wastewater from the liquid organic fertilizer plant. *Sep. Purif. Technol.* **2013**, *112*, 11–19. [[CrossRef](#)]
36. Garcia, J.C.; Takashima, K. Photocatalytic degradation of imazaquin in an aqueous suspension of titanium dioxide. *J. Photochem. Photobiol. A Chem.* **2003**, *155*, 215–222. [[CrossRef](#)]
37. Nikazar, M.; Gholivand, K.; Mahanpoor, K. Photocatalytic degradation of azo dye Acid Red 114 in water with TiO₂ supported on clinoptilolite as a catalyst. *Desalination* **2008**, *219*, 293–300. [[CrossRef](#)]